# Recent Results of T-10 Tokamak.

V.A. Vershkov 1) for T-10 team

*1) RRC "Kurchatov institute", Moscow, Russia.*

E-mail: vershkov@nfi.kiae.ru

**Abstract.** Poloidal asymmetry and radial correlation lengths of turbulence were investigated at LFS and HFS by means of correlation reflectometry. Correlation of the plasma confinement with the turbulence type was observed. Improvements of Heavy Ion Beam Probe diagnostic enabled to measure plasma potential in a set of regimes in wide radii range. The turbulence appeared to rotate close to [E×B] velocity. The concept of the ITB formation at the low order rational surfaces under the conditions of the low density of the rational surfaces was proved by the observation of the ITB formation near q=1.5 region with the use of non-central ECRH heating and current ramp up. The kinetic phenomena were investigated by ECE under strong central ECRH. Lithium gettering of the limiter and the wall give possibility to reduce significantly impurity level and recycling coefficient up to 0.3. The rates of carbon film deposition were measured in working and cleaning discharges. Second harmonic EC assisted start up was investigated in T-10. Possibility of the control of runaway electron generation and current decay rate after an energy quench at the density limit disruption was shown using ECRH.

## 1. Introduction

The T-10 experiments were carried out in Ohmic and ECRH discharges. The main topics of investigations were the physics of the core anomalous transport of different plasma species, the core and SOL variations under the Li gettering and studies of second harmonic EC assisted discharge start up. The characteristic features of the core investigations were the use of the wide variation of the ECRH radial power profile, the full coverage of the radial and poloidal turbulence distribution with the correlation reflectometry and the measurements of the plasma potential by HIBP.

## 2. Spatial Structure of Small Scale Density Fluctuations Study in T-10 Tokamak with Correlation Reflectometry

The identification of the physical mechanisms of the small-scale turbulence is the important topic of the investigations of the anomalous plasma transport. The review of the experimentally observed at the low field side (LFS) turbulence types in T-10 can be found in [1]. The first results of turbulence investigation at the high field side (HFS) revealed strong poloidal turbulence asymmetry [2].The characteristic features of LFS spectrum are the presence of the maxima near 70, 150 kHz and zero frequency and significantly higher level with respect to HFS. These maxima were referred to as low and high frequency quasi-coherent (LF QC / HF QC) and stochastic low frequency (SLF) respectively. It was shown [1] that characteristics of LF QC are similar to the predicted by theory for ion temperature gradient (ITG) instability and HF QC to trapped electron mode (TEM).

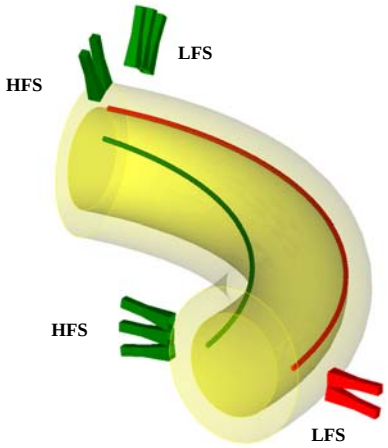


*FIG. 1. Schematics of the reflectometry antenna arrays positions on T-10.*

Present studies were devoted to the detailed investigation of the spatial structure of the turbulence with correlation reflectometry [1]. New antenna array was installed at LFS

with that aim. The final scheme of T-10 antenna array is shown in Fig. 1 (new antenna marked by red). It makes possible to measure: 1) the whole poloidal turbulence asymmetry from 4 poloidal angles; 2) radial correlations at LFS and HFS; 3) long distance toroidal correlations along the magnetic field line at LFS and HFS (as shown in Fig.1 by lines); 4) turbulence variation at HFS/LFS under different densities and currents. Although all items are in progress, this paper deals only with two first topics, because the last two need additional work and will be published elsewhere.

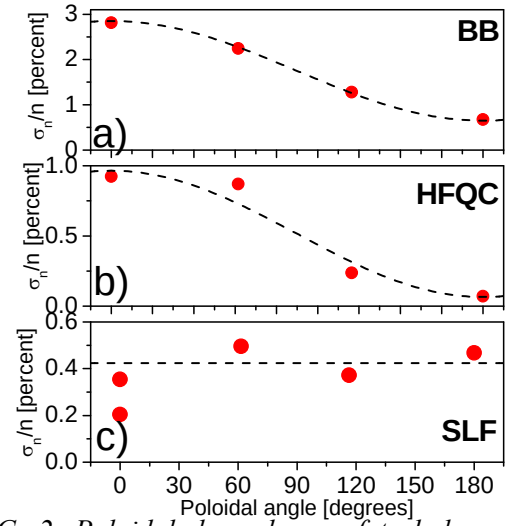


*FIG. 2. Poloidal dependence of turbulence levels for different fluctuations types.*

The poloidal variations of different turbulence types are presented in Fig.2. Experiments were carried out in OH discharge with $I_p$=250 кА, $B_T$=2.4 T and $n_e$=2.7·10$^{19}$ м$^{-3}$ at the radius of about 2/3 of plasma minor radius. The highest asymmetry (13) is observed for HF QC (Fig.2b), BB turbulence level has asymmetry about 4 (Fig.2a) and SLF fluctuations (Fig.2c) do not depend on poloidal angle. So one can conclude that the quasi-coherent feature is practically localized only at LFS, as predicted by 3D gyrokinetic codes for the drift waves [3]. But the high asymmetry of the HF QC raises the question about lower asymmetry of the BB, because earlier [1] both phenomena were regarded to have the same physical mechanism. The first question was to investigate the difference in the properties of the BB at LFS and HFS. The second question was connected with the radial localization of SLF feature. As SLF have rather long radial and poloidal correlation lengths [1], so O-mode reflectometry measurements in the core regions will be no more local, because they will be greatly influenced by the high turbulence level at the edge.

### 2.1. Radial correlation measurements

In order to clarify both questions, detailed radial correlation measurements were carried out in similar discharges at LFS and HFS with the correlation of the O-modes and O-mode with low frequency extraordinary XL mode. In addition BB and SLF features were explored in experiments with Amplitude Modulation (AM) reflectometry and long distance toroidal correlations. New measurements of the radial correlations with two O-mode reflectometers for HFS and for LFS presented in Fig.3 (top and bottom panels respectively). Experiments were carried out in similar regimes with magnetic field $B_T$=2.4 T, plasma current $I_p$=250 kA and density about 1.6×10$^{19}$ m$^{-3}$. Two heterodyne reflectometers were used with frequency ranges from 36 to 55 GHz and from 25.5 to 37 GHz, which had overlapping

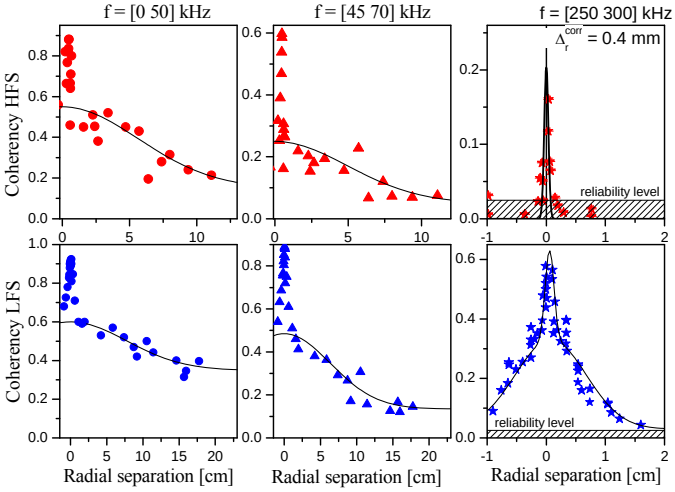


*FIG. 3. Radial cross-correlation functions for different frequency bends at HFS (top) and LFS (bottom).*

frequency range from 36 to 37 GHz. It was found experimentally that the minimal possible frequency difference was 80 MHz due to the significant cross-talk between two reflectometers, resulting in unstable work. The frequencies were constant during the discharge and were changed from one to another pulse. Figure 3a show the coherency dependence on the distance between reflecting layers for the low frequency band at HFS. Sharp initial decrease, attributed to BB, changes to the slow decrease with $\lambda_r$ = 7.5 cm, and some residual background, which is typical for SLF. The further evolution of the correlation function with the increase of the frequency band can be seen in Fig.3. One can see the relative decrease of the SLF feature with frequency band rise and its final disappearance at frequency band higher 100 kHz. One can see also that very narrow peak with the $\lambda_r$ = 0.4 mm exists in all frequency bands, but became the only one at the high frequency band. The long correlation length for SLF just confirm our previous results [1], but the new experimental correlation length for HFS BB was in a order of magnitude less then at LFS and raises the question about reflectometry radial resolution. Such correlation length was about 1/20 from the probing reflectometry wavelength. 2D full-wave modeling in real T-10 geometry with random Gaussian perturbations with width of 3.5, 2.5 and 1 mm gave the equal correlation lengths of about 7 mm, irrespectively from the perturbation width in accordance with the theory [4].

This question stimulated the new experiments at LFS in exactly the same conditions. Antenna array LFS A at 60 degrees to equatorial plane was used to reproduce our previous results and for technical reasons (see Fig. 1). The results for the LFS are presented in Fig. 3 (bottom panels) from low to higher fluctuations frequency bands respectively. Qualitatively the results at LFS are similar to the HFS. There are two main features – SLF turbulence with long correlation lengths which dominates at low frequency bands and short correlated BB feature, dominated at higher frequencies. But there are significant difference of LFS correlations with respect to HFS ones. Firstly the SLF turbulence has very long correlation lengths. At low frequencies SLF correlated practically over the whole column, which may suggest the lack of locality of reflectometry for the long wavelength turbulence. Secondly, one can see in all frequency bands that BB at LFS has two distinct components (see Fig. 3 bottom, right): very narrow peak with the $\lambda_r$ = 1 mm on the top of the wider correlation function with $\lambda_r$ = 3.5 mm. The former looks like the HFS BB and gives about 40% contribution to the total correlation value, and the later is the special feature of the LFS and its contribution about 60%. Taking into account the BB asymmetry 2.5 (see Fig.2 for the poloidal angle 60°), one may formally suggest that there are two different turbulence components: symmetrical poloidally short correlated component with $\lambda_r$ = 1 mm (40% at LFS) and specific only

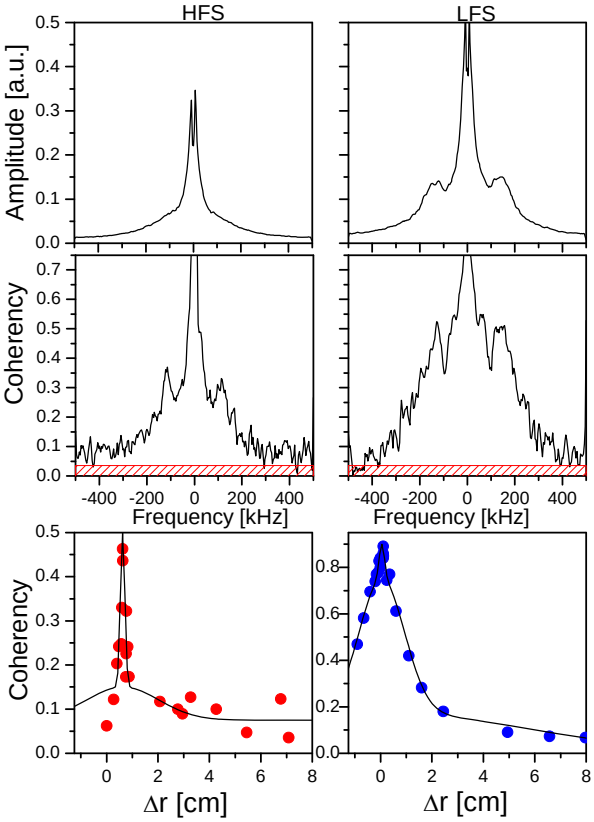


*FIG. 4. The signal Fourier of spectra (top) and radial coherency (middle) for HFS (left) and LFS (right). Red shaded regions on the middle plots show confidence level. Radial coherency function at frequencies 90 - 150 kHz (bottom).*

for the LFS component with $\lambda_r$ = 3.5 mm (60% at LFS). This accounts for the integral BB asymmetry 2.5. But in any case such formal decomposition can't explain experimental fact of observation of extremely short correlation lengths. It was already mentioned that 2D model simulation with Gaussian perturbations can not explain $\lambda_r$ shorter than 7 mm. But in accordance with theory, it is possible to expect shorter $\lambda_r$ with oscillatory perturbations [4]. In fact for the HFS such perturbations are predicted in 3D gyrokinetic simulations [3] due to the toroidal coupling of the perturbations at the high order rational surfaces in condition of non-zero magnetic shear [1]. In such conditions the radially elongated structures at the equatorial LFS (which was associated in [1] with quasi-coherent turbulence) transformed to the two sets of highly spiral structures at HFS. Thus forming oscillatory perturbations with about $\lambda_r \cong 1$ mm. This hypothesis is confirmed by the experiments with long distance toroidal correlations at the HFS [2]. It was shown that correlation length of the QC turbulence are large than one turn around the major tokamak axis. In given experimental conditions value $q < 2$ means that the HFS/LFS connection length L is less than $2\pi R$. The presence of the maxima of the LF QC at frequency about 120 kHz in coherency spectra are clearly seen at LFS and HFS in Fig. 4. While the coherency spectra look similar, the amplitude spectra are different. And the radial correlation lengths for the frequency band around 120 kHz (shown in Fig.3, bottom panels) differ in an order of magnitude. Those facts are in good agreement with the toroidal modes coupling hypothesis. The natural question about the mechanisms of transformation rather defined QC frequency into wide frequency range BB should be considered. The case is that at the LFS the QC structures are elongated radially and their frequency is determined by the Doppler mechanism due to plasma rotation. In contrast at HFS there are complex structure with two sets of the spiral QC. So the structures become significantly stretched poloidally and formed oscillatory perturbations radially with two signs of helicity. In additional the experiments with long distance toroidal correlations at the HFS [2] and new experiments at LFS showed that QC fluctuations are traveled as the drift turbulence at the angles inside +/- 0.5° to the magnetic field line. This fact will result in the additional stochastisity of QC at HFS after travelling the distance about 10 m from LFS to HFS. It is natural to consider the application of the same mechanism for the formation of BB at LFS. In this terms the 40% shortly correlated part corresponds to the QC coming toroidally from long distances, compared with one toroidal turn, while the 60% with $\lambda_r$ = 3.5 mm arise from the fluctuations originated from the more close regions at LFS. Due to the lower connection length they have less helicity and higher $\lambda_r$. Finally the QC fluctuations originated near the observation location will be seen like QC with the definite maximum in the turbulence spectrum. Of cause the considered hypothesis did not exclude the possibility of the two different turbulence: symmetrical poloidally with short correlation length ($\lambda_r \cong 1$ mm) and specific only for the LFS fluctuations with $\lambda_r \cong 3.5$ mm.

### 2.2. Characteristics of Stochastic Low Frequency turbulence

The SLF turbulence covers the frequency band from several to 100 kHz in the turbulence spectrum. The main property of SLF is the poloidal uniformity (see Fig.3d) and the radial correlation length about 6-10 cm (Fig. 4). The poloidal correlation measurements enabled to estimate characteristic poloidal dimensions also about 5 cm. So such long wave fluctuations may be treated in 1D approximation. It is well known that the relative density fluctuations at plasma edge in OH and L modes may reach 10 – 50% and their spectral maximum is just in the low frequency band [1]. Thus it should be considered the case that all SLF turbulence is originated from the edge. In order to estimate the edge turbulence effect on the radial correlation measurements 1D model simulations were performed. Strong edge turbulence (dn/n=10%) at the limiter was superimposed with core (dn/n=0.5%). The modeling were

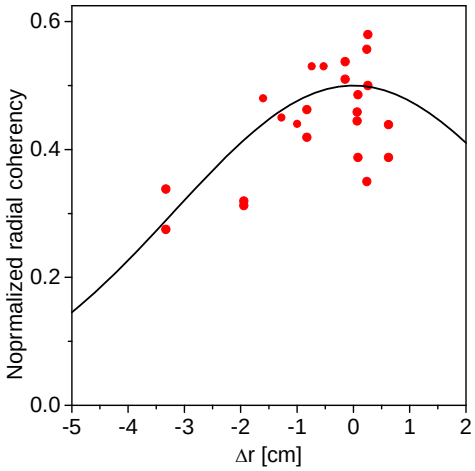


*FIG. 5. Correlation at HFS of O-mode at 51 GHz and XL mode (around 25.5 GHz) in a frequency band 20-50 kHz*

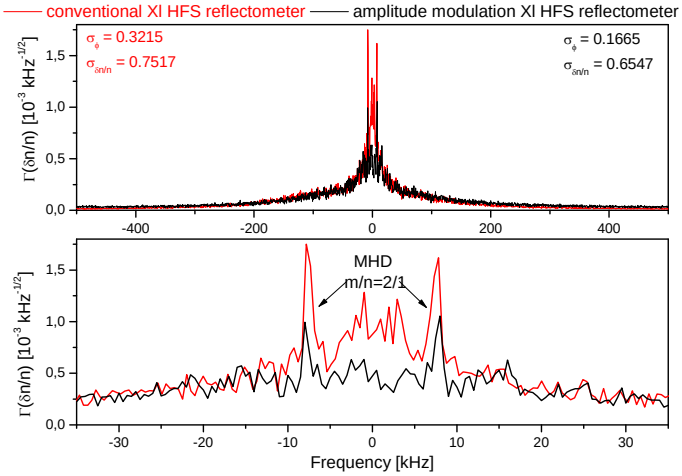


*FIG. 6. Fourier spectra of conventional (red) and AM (black) reflectometers at HFS. Bottom plot – zoom low frequency region of spectra.*

performed for radial correlations of two O-modes, O-mode with XL mode, correlations of two XL modes and the correlations of two Amplitude Modulated (AM) XL modes. It was found that correlation of the two O-modes is the worst case. The correlations of the O and XL mode is much better. It should be mentioned that the low sensitivity of the XL mode to the edge fluctuations is the specific feature of this mode. The correlations of the two XL modes makes situation much better and correlations of the two AM modulated XL modes is the best. So according to the simulations significant improvement of SLF radial localization may be obtained by the correlations of O and XL modes, which was carried out experimentally at the HFS. The discharge parameters were close to the discharge with the radial O-mode correlations, except the higher density Ne= $2.5\times10^{19}m^{-3}$. Reflectometry with O-mode had the frequency range from 36 to 55 GHz, and for XL mode from 25.5 to 37 GHz respectively. The reflection layer was around 20 cm. The result of such experiment at HFS is presented in Fig.10. One can see that in accordance with the simulations, the localization of SLF turbulence became much better with $\lambda_r$ = 4.5 cm. The further improvement of the SLF localization may be achieved by the application of amplitude modulation of XL mode with the frequency $F_{mod}$=80 MHz. Conventional reflectometry measures the fluctuations of the phase of the main launched wave. In contrast the AM reflectometry measures the phase fluctuations of the wave envelops. The resulting spectra for the conventional XL HFS reflectometry and AM XL one are compared in Fig.6. Thus the experiment improvement enables to prove the existence of SLF at the HFS in the core region with the radii less than 2/3 of the limiter.

Additional evidence of the core SLF were obtained during long distance toroidal correlation experiments at HFS and LFS. SLF fluctuations was found at HFS with radius of 16 cm [2], while SLF were not detected at the LFS at the radius 21.5 cm. So these results additionally proved the core SLF location with the radii less than 2/3 of the limiter (20 cm). The correlation reflectometry measurements with XL mode were performed in FTU tokamak with similar dimensions [5]. The SLF turbulence was clearly seen in these experiments. So we can conclude that SLF turbulence is present in core regions of tokamaks at HFS and LFS. The SLF turbulence had constant phase along the magnetic field line [2], which is typical either for the magnetic or interchange turbulence.

### 3. Correlation of plasma transport with turbulence type.

The experiments of the transport studies of different plasma species, including impurity, and ion and electron heat transport in correlation with turbulence characteristics were carried out in T-10 ohmic discharges with different plasma parameters [6]. The experiments were carried out with a line averaged plasma densities varying in the region of $0.4<n_e<5.6*10^{19}m^{-3}$ in Ohmic plasmas. Diffusion of He ions and ion temperature profiles were measured with the recently became available CHERS diagnostic using the diagnostic hydrogen neutral beam. At low density low frequency quasi coherent (ITG) is a dominant mode. Intermediate densities are characterized by the presence of high frequency quasi coherent (TEM) modes. Argon confinement times ($\tau_{Ar}$) have been obtained from evolution of $Ar^{+16}$ line radiation in steady-state discharges after short gas puff. Confinement of He impurity was found to be close to that of argon. The measured $\tau_{Ar}$ does not depend on density in a wide range of intermediate densities and decreases strongly at low density, where ITG turbulence became dominant. Also good agreement of the central ion temperature value with the neoclassical "Artsimovich expression" [7] was found at the intermediate densities, while significantly lower temperatures were measured with the density decrease [6]. At high densities the increase of the gas influx resulted in the degradation of confinement and decrease of the ion temperature. The degradation of confinement also accompanied by the turbulence transition from TEM to ITG mode. Under the decrease of gas influx the confinement and increase of both the ion and the electron temperatures occurs together with turbulence back transition from ITG to TEM. So experiments showed the good correspondence of the ion confinement degradation with the developments of ITG instability at low densities and high influx discharges at high density.

### 4. Measurements of plasma potential, radial electric field and turbulence rotation velocity in the T-10 tokamak

The absolute value of the core plasma potential φ and its fluctuations were measured by Heavy Ion Beam Probing (HIBP) diagnostic [8,9]. The $Tl^+$ beam energy of HIBP was increased up to $E_b$ = 300 keV, and the beam current up to 200 μA. This allows to observe the core potential at high densities and in a wide radial area for the first time. The regimes with Ohmic (OH), on- and off-axis Electron Cyclotron Resonance (ECR) heating ($B_t$ = 1.55–2.4 T, $I_p$ = 140-250 kA, $\bar{n}_e = (1.3 - 4.1) \times 10^{19}$ $m^{-3}$, $P_{EC}$ < 1.5 MW) were studied, see Table 1. The φ(*r*) profile presents linear-like function and the slope of the profile allows to estimate the mean radial electric field $E_r$: The potential well becomes deeper, and $E_r$ becomes more negative with the rise of density and energy confinement time $\tau_E$. This result is consistent with earlier measurements in TM-4 [10] and TJ-II [11].No strong irregularity has been observed on the φ(*r*) profile at the area of ECRH power deposition. The broadband turbulence rotation velocity $\Omega_{TURB}$ was measured by CR in the regimes I and III at the same discharges as HIBP. Figure 1 (a,b,c) shows that $\Omega_{TURB}(r)$ is close to $\Omega_{E\times B}(r)$ in the whole observed radial, density and toroidal magnetic field ranges both in OH and ECRH plasmas. Thus it is possible to

| *Regime* | $\bar{n}$, $10^{19}$ $m^{-3}$ | $E_r$, *V/cm* | *Δr, cm* | $B_t$, *T* | $I_p$, *kA* | $\tau_E$ , *ms* |
|---|---|---|---|---|---|---|
| *I* | *1.3* | *55* | *6-30* | *1.55* | *140* | *20* |
| *II* | *2.4* | *65* | *6-30* | *1.55* | *140* | *36* |
| *III* | *2.5* | *70* | *7-22* | *2.08* | *165* | *38* |
| *IV* | *4.1* | *90* | *16-27* | *2.4* | *210* | *50* |

*Table 1. Parameters of discharges that were studied by HIBP and CR.*

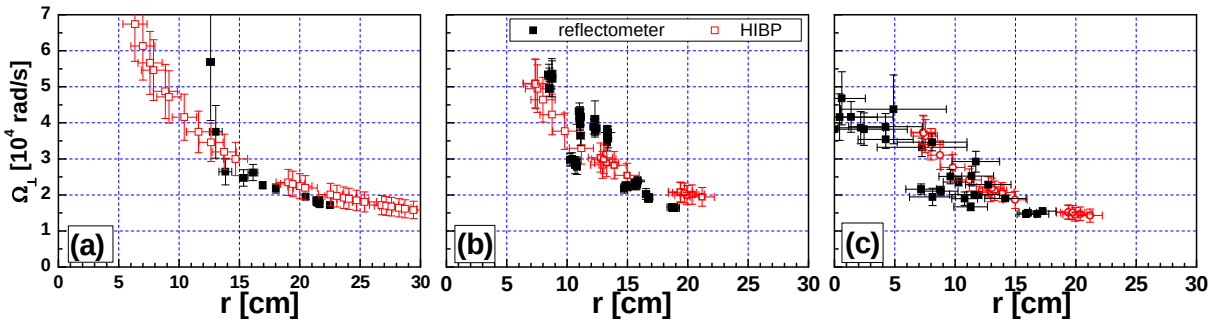


*FIG. 7. Comparison of rotation velocities of density perturbations $\Omega_{TURB}$ from CR, with core plasma rotation $\Omega_{ExB}$ from HIBP in OH (a – $B_T$=1.55 T; b – $B_T$=2.08 T) and ECRH (c) plasmas.*

conclude that within the experimental accuracy turbulence does not have any additional intrinsic rotation in the frame of E×B.

## 5. **Studies of role of the rational surface density and self-organized pressure profile.**

From previous experiments it is known, that ITBs are formed in the regions with very low or zero rational surfaces densities [12,13]. It has been noted in [13] that in the vicinity of low-order rational surfaces there are gaps where modes with number *m/n* do not exist. In such gaps the turbulent cells are physically separated and electron ITBs can be formed in such gaps. In order to check the role of rational surface density in the process of eITB formation it was carried experiments, which permitted change strongly the density of the rational surfaces. Off-axis ECRH was used to suppress sawteeth oscillations and then the plasma current was rapidly ramp with the rate up to 3 MA/s during 15 ms from $I_1$=160 kA to $I_2$=206kA [14]. The suppression of sawteeth oscillation and current ramp-up produce more flat *q* profile in vicinity of rational surface *q*=1.5 and forms the region with low density of the rational surfaces as one can see in Fig.8 a,b. Thus the electron ITB appears in the vicinity of rational surface *q*=1.5 after off-axis ECRH beginning and ITB improves after the current ramp-up. Temperature time evolution inside (r=13.5 cm) and outside (r=23 cm) eITB region are shown in Fig.9.

The analysis of the experiments showed that the conservation of self-consistence pressure profile *pN*(*r*) occurred in the regions where the turbulent cells overlap and can be violated in the opposite case. Low electron heat conductivity in ITB zone created by the off-axis ECRH was additionally analyzed by means of heat pulse propagation (HPP) [15]. A slow HPP propagation, corresponding to $\chi_e^{HP}$ =0.08 m$^2$/s was observed.

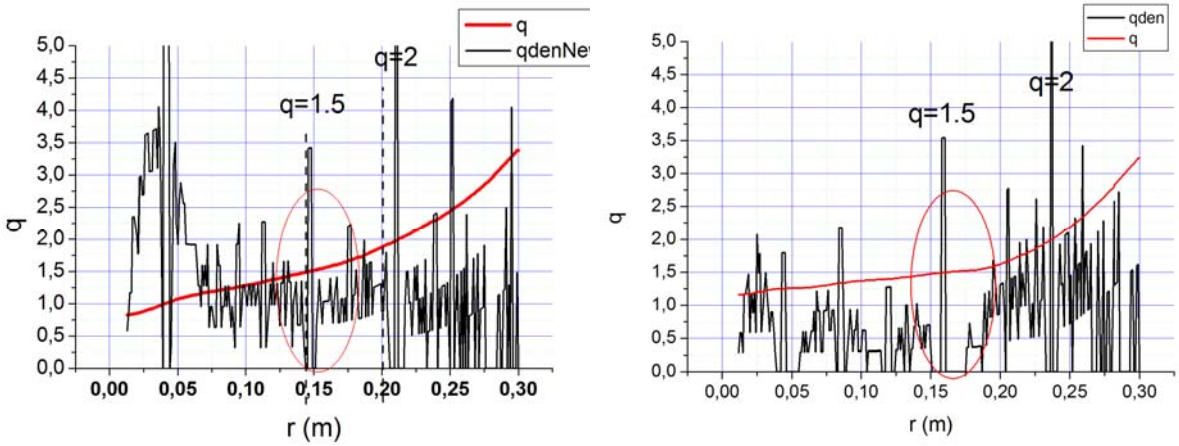


*FIG. 8. ASTRA calculation of q(r) profile and the density of rational surface at Ohmic stage (a) and after off-axis ECRH and current rump-up (b).*

## 6. Investigation of kinetic effects in plasma by means of ECE

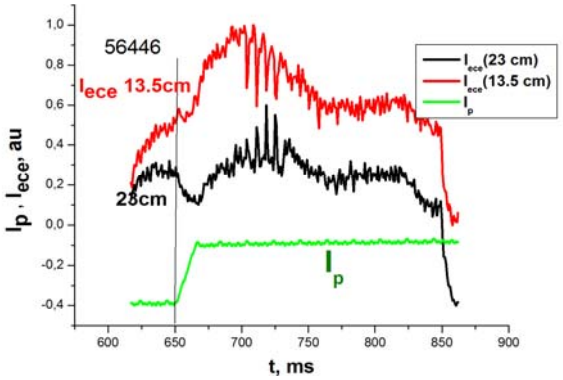


*FIG. 9. Temperature time evolution inside (r=13.5 cm) and outside (r=23 cm) eITB region. (Off axis ECRH starts at 650 ms). One can see, that temperature gradient is raised after ECRH start and increases after current ramp-up.*

Main method for the investigation of kinetic phenomena in T-10 plasma experiments is ECE diagnostic with high space resolution (about 1 cm). The system includes multi-channel receivers and permits to measure an emission either in the first or in the second ECE harmonics. The fast frequency scanning system is also used for investigation of the ECE spectra simultaneously in two polarizations. Diagnostic complex includes also measurements of plasma electromagnetic noises in range of magnetized Langmuir oscillations (0.5 - 24 GHz). They are measured by small loop antennae insulated from a direct contact with plasma. Emission of the extraordinary wave is determined only by perpendicular electron energy, while an emission of the ordinary wave depends also on the longitudinal energy. According to the linear theory both polarizations are identical for the electron temperature measurement, provided high optical depth. Different dynamics of signals should point out directly to non-Maxwellian electron distribution. Fig. 10 shows ECE signals in both polarizations from the same plasma volume in the central plasma zone (r = 5 cm) where optical depth is enough high. High power on-axis ECRH (~1.2 MW) intensifies the global oscillations in mode m/n=1/1. The experiment showed that oscillations of O-ECE in m/n=1/1 mode are shifted in ~45 μs with respect to X-ECE. Considerably different dynamics of signals remains up to the end of ECRH. We can say confidently that distribution function widens and compresses periodically in two time scales: in every period of m/n=1/1 oscillations (f~3.5 kHz) and during overall sawtooth cycle. The evaluation shows that the longitudinal velocity oscillates more strongly than perpendicular one though ECRH inputs power only in the transverse electron energy. The background level of plasma noises rises quickly with start of ECRH and finally exceeds the OH level in a factor of two. Strong simultaneous spikes at every internal disruption (and small disruption) can surpass a background more than one order of magnitude. Supposing that the measured electromagnetic noise originated from the small scale potential plasma waves due to conversion mechanism, one may conclude that plasma waves are exited in stationary

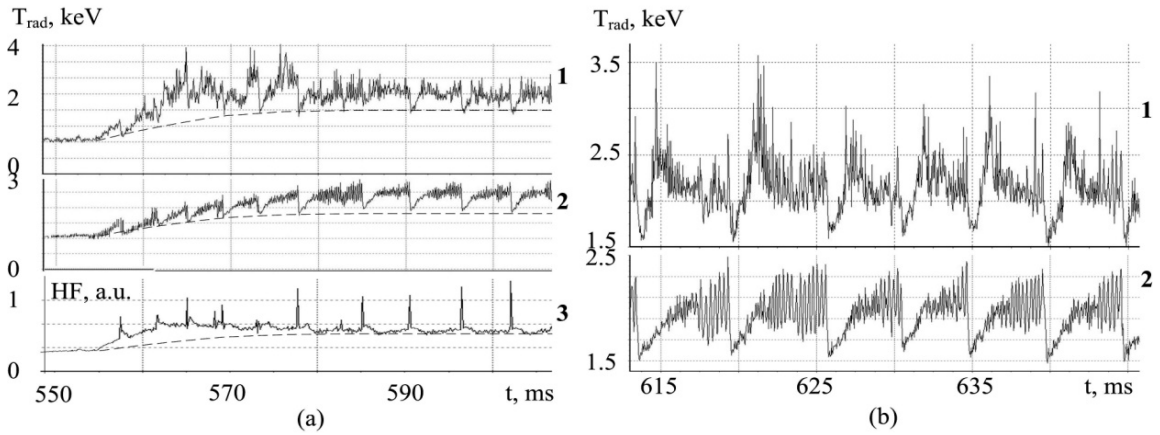


*FIG. 10. ECE in 1st O-mode (1) and in 2nd X-mode (2): (a) – first stage of ECRH, HF – plasma noise signal (3) by receiver with frequency range 1 – 16 GHz; (b) – steady-state stage of ECRH.*

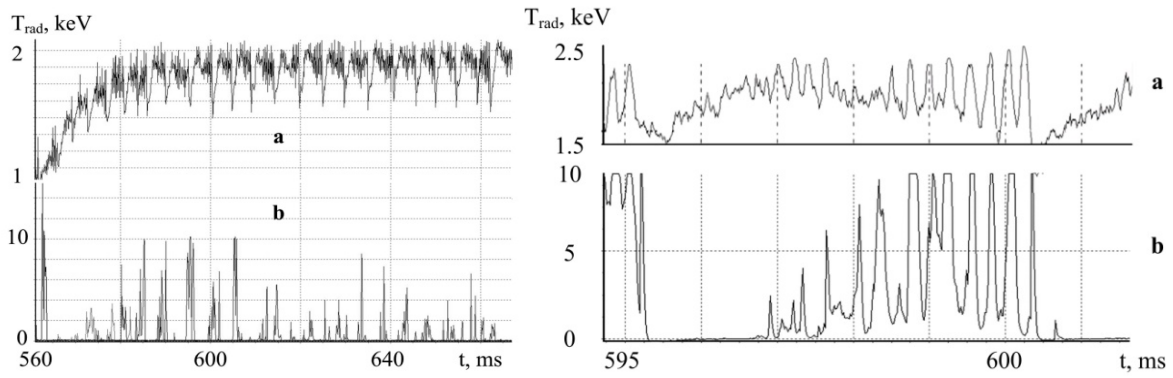


*FIG. 11. ECE signals by X-mode (a) from the center (134 GHz, 5 cm) and O-mode (b) from the column periphery (41 GHz).*

and transient conditions and their role in fast non-local transport processes should be considered.

Besides the strong oscillations of the main part of plasma electron function at the column center the intense oscillations of the first O-mode ECE harmonic at the extremely low frequencies (formally corresponding to the radii outside the limiter) always was aroused in the first stage of the on-axis heating. Such emission may be interpreted as the downshifted ECE created at the edge by the high energy component of electrons (190 – 220 keV). Fig. 11 illustrates such O-mode ECE emission oscillations measured at the frequency 41 GHz. Similar emission was also observed for X-ECE but they are smaller more than one order of magnitude. It means that high energy electrons had mainly longitudinal energy. Bursts of the periphery ECE emission oscillations occurs synchronously with the central oscillations in m/n=1/1 mode. It should be noted that observation of the edge downshifted ECE emission became impossible at high periphery density, because in this case the position of O-mode wave cut-off layer is in the SOL region and screens edge ECE emission. Edge localization of downshifted ECE emission was proved by means of edge density variation. The bursts of the high energy electrons supposed the strong pulsed longitudinal electric field up to ~1 V/cm. Such fields may be produced by the plasma current relaxation at the central plasma area (mode m/n=1/1). The synchronous behavior of the bursts at the plasma core and boundary shows apparently strong coupling of the core and edge plasma, which can be caused by the potential plasma waves.

## 7. Experiments with lithium gettering in T-10

Lithium gettering of the limiter and the wall give possibility to reduce significantly impurity level and recycling coefficient up to 0.3. The review of the first results of the experiments with lithium gettering were presented at the 2008 IAEA Conference [16]. The recent results concerned with the detail analysis of the Li distribution over the rail limiter and the estimation of the absolute Li outflux by means of Li pellet injection. One of the characteristic feature of the Li behavior in T-10 is the very slow Li migration along the tokamak chamber. There were four T-10 campaign with 14 Li gettering. The estimated total amount of Li introduced into the chamber was about 20 grams. But neither spectroscopy, no chamber inspection after venting detected any Li traces at the chamber side, opposite to Li getter. This phenomenon definitely connected with the high efficiency of the Li screening by the limiters. The quantitative analysis of the Li distribution over the surface of the rail limiter after venting was carried out. As Li after two weeks of exposure to atmosphere converts to the final white dust of $Li_2(CO_3)$, so its distribution was estimated by the degree of local “whiteness”. The evidence of the high

screening of the circular limiter is the rapid decay of the density of Li dust in the shadow of the circular limiter with characteristic decay length of 11 mm. It corresponds to the decrease of Li density in a factor of 100 at the wall in the 50 mm limiter shadow. The absolute Li outflux was estimated by means of the injection of Li pellets by pneumatic gun. The increase of the plasma density and the decay rate was controlled by eight channel interferometer. Assuming that all density increase and the density decay was due to Li, it was possible to calculate the outflux of the Li from plasma. As the experiments showed that in stationary conditions Li influx was significant only near the limiter (where evaporation was made), so the brightness of the Li lines away from the limiter should be determined only by recombination of Li outflux. Thus the relative increase of Li lines give information about the stationary Li outflux. The lithium outflux was calculated from the decay rate of the total number of particles after injection. The value of integral Li ions outflux was $2\times10^{20}$ ions/s. This value was approximately 10% of the integral deuterium influx. Assuming the equal penetration probability of Li and D to the core one can estimate $Z_{eff}$ about 1.6. As the experimental value of $Z_{eff}$ = 1.1-1.2 [16], the penetration probability of Li in a factor of 3-6 lower than that of deuterium. It should be noted that the real Li penetration probability must be much lower, as carbon and iron [16] still must be the main contributors to $Z_{eff}$.

## 8. Experiments with film deposition in T-10

The spattering of the limiters and co-deposition of the carbon and tritium are the important problems for the tokamak-reactor. The redeposition of the carbon, sputtered from the graphite limiters was investigated on the T-10, by exposure of the mirrors and samples in the different points of the SOL. Redeposition was investigated separately in working as well as in cleaning discharges of T-10. Composition of the films was measured using EPMA technique. Surface structure and morphology were investigated by optical and electron microscopes and by profilometer. Thickness and optical parameters (refractive index and extinction coefficient) of the films were estimated by ellipsometry. For the working discharges the deposition rate was 0.08 nm/sec at the position far (about 2.5 m.) from the graphite limiters. But it was increased up to 0.5 nm/sec more than order of magnitude in a close vicinity to the limiter. The deposited films are amorphous and consist from carbon and hydrogen (with typical ratio 3/1- 2/1) without any metallic species. For the cleaning discharge deposition rate was 0.008 nm/sec that is more than order lower than for the working one. But due to the long duration it contributes strongly to the total redeposition of the sputtered carbon. The films surface was observed with Atomic force microscope. The results in working and cleaning discharges are presented in Fig.12 a, b, respectively. It is clearly seen the significant difference of the films surfaces in two cases. In working discharges the deposited film have the feature of the globular structure, while such feature practically absent for the cleaning discharges.

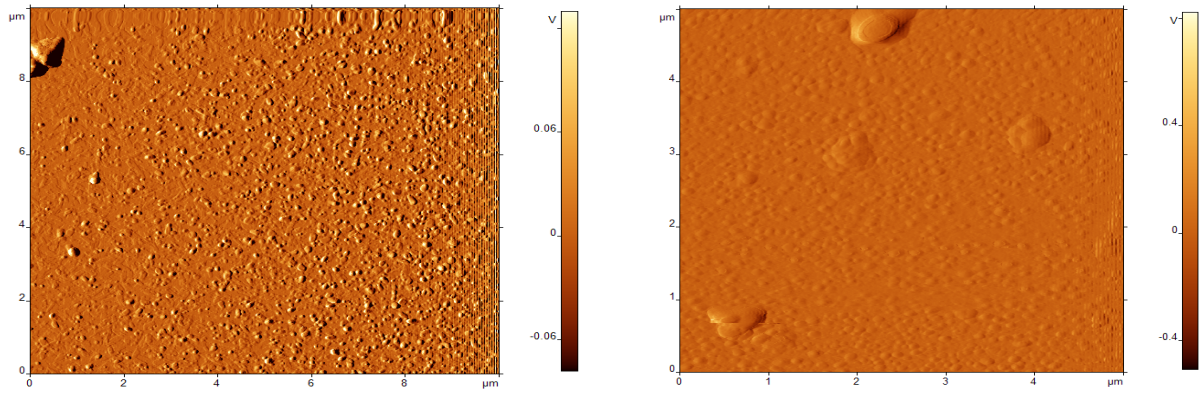


*FIG. 12. Left - globular structure of the film, deposited in working discharges; right - smooth structure of the film, deposited in cleaning discharges. Atomic force microscope data.*

**9. Investigation on runaway electrons control.**

Present experiments in the T-10 tokamak has demonstrated possibility of the control of runaway electron generation and current decay rate after an energy quench at the density limit disruption using ECRH heating in combination with preprogrammed Ohmic power supply system and gas puffing. Essential new result of the present experiments is identification of the optimal conditions of safe termination of the plasma discharge using auxiliary heating and identification of the nonthermal x-ray perturbations at the initial stage of the current collapse using 2D CdTe tomographic arrays.

**10. ECR-assisted breakthrough experiments.**

Problem of pre-ionization and ECR-assisted start-up is widely discussed now due to the importance of the beginning stage of discharge in ITER. It is known that ITER construction leads to restriction of toroidal electric filed at the level about 0.3 V/m so pure Ohmic burnthrough become impossible or exist only in a very narrow interval of initial parameters. Previous T-10 experiments demonstrated significant decrease of loop voltage when ECR at the 2nd harmonic of electron cyclotron resonance is applied to working gas before the start of discharge. Recent experiments were pointed on the physical mechanism of microwave induced pre-ionization and optimization of parameters to achieve best plasma parameters. ECR-only heated plasma was investigated to reveal the nature of observed effect and exclude the influence of loop voltage on the phenomena. Toroidal magnetic filed in experiment was about 2.0-2.6 T and working gas initial pressure was $(4.5\div6)\times10^{-3}$ Pa. Microwave power was launched at frequency 140 GHz and total power was up to 0.95 MW. It was made a special experiment concerning position where the plasma column begins to from. 16-channel interferometer was used to observe the radial profile of plasma electron density. The resulted spatial distribution of integral density is shown in Fig. 13. It is clearly seen that plasma initiation begins at the position of cold cyclotron resonance. Experiments demonstrated existence of two regimes after burnthrough where only 0.45 MW ECR power and vertical magnetic field were applied to the discharge. First one is characterized by absence of the toroidal current, the second one has toroidal current about 3-8 kA (Figure 14). Discharges with non-inductive toroidal current were achieved when estimated total vertical magnetic filed was $(1\div2)\times10^{-3}$ T. The nature of this current is the equilibrium currents that flow along the plasma and short through vacuum vessel. It was found that regimes without toroidal current had narrow electron density and visible lines intensity profiles (figure 15left column) with maxima at the electron cyclotron resonance position. Discharges with equilibrium current had rather wide profiles, higher visible light emission and significant burn-through of highly-ionized carbon ions in plasma center (figure 15, right column). An estimation of electron temperature was made in both types of discharges using coronal model of light emission carbon ions. It was found that in discharges without toroidal current electron temperature was about 5-10 eV, whereas best discharges with current electron has temperature up to 150 eV and electron density $0.5\times10^{19}$ m$^{-3}$. Thus the discharges with

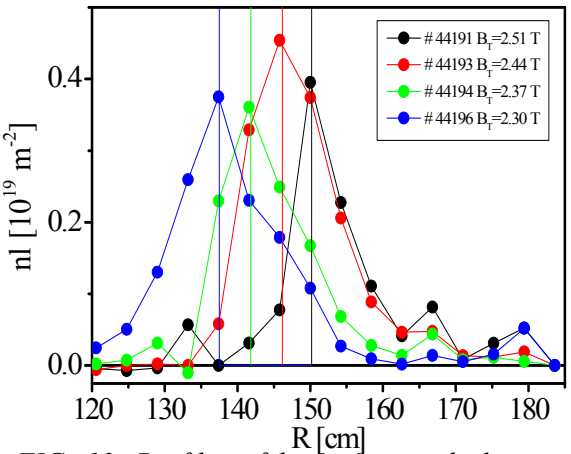


*FIG. 13. Profiles of line integrated electron density in ECR assisted discharges with different toloidal magnetic field values. Vertical lines show cold resonance positions.*

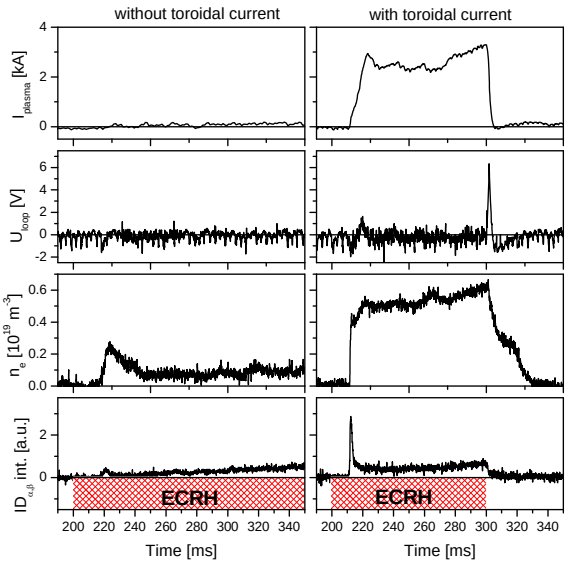


*FIG. 14. Time traces of main plasma parameters in ECR assisted start-up discharges. Left ones – without toroidal current; right ones - with toroidal current. Parameters (from top to bottom): toroidal plasma current, loop voltage, line-averaged electron density, $D_\alpha$ line intensity.*

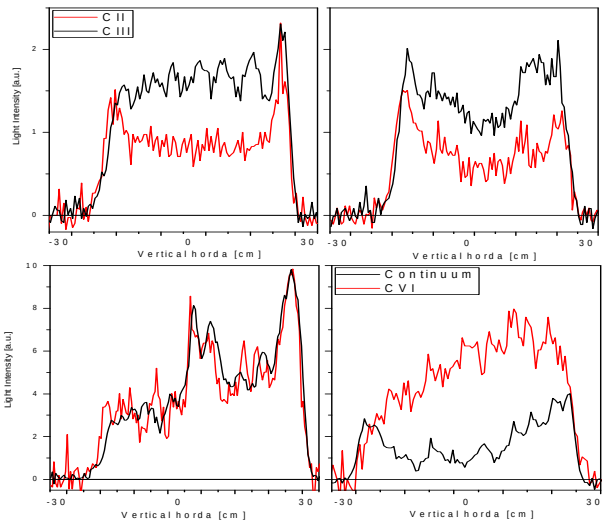


*FIG. 15. Comparison of light intensity profiles for CII u CIII lines (top); CVI and recombination continuum (bottom). Left curves correspond to case without non-inductive toroidal current; right one – to the case with toroidal current.*

equilibrium currents formation are looked as the best candidate to further current rump-up.

This work is supported by Rosatom Contract H.4f.45.03.10.1009, Rosnauka Contract 02.740.11.5062 and Grants RFBR 08.02.01326, RFBR 08.02.90468, NWO-RFBR 047.018.002.

References

[1] V.A. Vershkov, D.A. Shelukhin, S.V. Soldatov, *et al*, Nuclear Fusion, 45 (2005), pp. S203-S206.
[2] D.A. Shelukhin, V.A. Vershkov, A.V. Khmara, et al, Proc. of 22nd IAEA Fusion Energy Conference, Geneva, Switzerland , 2008, IAEA-CN-117/EX/P.5-37.
[3] Waltz R.E., Kerbel G.D., Milovich J. , Phys. Plasmas, 1994,V. 1, № 5, P. 2229-2244
[4] E. Z. Gusakov and B. O. Yakovlev,, Plasma Phys. Control. Fusion 44 (2002) 2525–2537
[5] A. Tuccillo, O. Tudisco, M. De Benedetti, *et al*, Proc. of 28th EPS Conference on Contr. Fus. and Plasma Phys., Madeira, Portugal, 2001, ECA Vol. 25A (2001), pp. 65-69
[6] N.Timchenko, V.Vershkov, V.Karakcheev, *et al*, 36th EPS Conference on Plasma Phys. Sofia, June 29 - July 3, 2009 ECA Vol.**33E**, P-5.196 (2009)
[7] L.A. Artsimovich, Tokamak devices. // Nuclear Fusion – 1972 – V **12** - p. 215 - 240.
[8] A.V. Melnikov et al., EPS 2010 – P1.056
[9] A.V. Melnikov et al., EPS 2010 – O5.128
[10] V.I. Bugarya et al., Nucl. Fusion 25, 1701 (1985).
[11] A.V. Melnikov et al., Fusion Sci. Techn. 31, 51 (2007).
[12] Joffrin E et al 2003 Nucl. Fusion **43** 1167
[13] Beklemishev A D and Horton W 1992 *Phys. Fluids* B **4** 200
[14] V.F. Andreev, this conference
[15] C.V. Neudatchin, this conference
[16] V.A. Vershkov, S.V. Mirnov, V.A.Evtikhin, *et al*,Proc. of 22nd IAEA Fusion Energy Conference, Geneva, Switzerland , 2008, IAEA-CN-117/EX/P.4-14